JOURNAL OF AIRCRAFT
Vol. 33, No. 5, September–October 1996

Directional Control of an Advanced Airship

Bellur L. Nagabhushan* and Swee B. Tan†
Saint Louis University, Cahokia, Illinois 62206

Directional control of a relaxed static stability airship is considered by means of an active control law. The yaw control moments from rudder deflection, differential thrust of two vectorable cruise/lift thrusters and a bow thruster device are integrated to synthesize an active control law that can be implemented in a digital fly-by-wire/light flight control system configuration. It is shown that significant improvement in airship directional control and maneuverability can be realized, especially at low airspeeds below 20 kn, by using the proposed active control law. Results are illustrated by considering an example 2.8-million-ft³ vehicle.

Nomenclature

a_t = tail aerodynamic lift curve slope, per rad
B = force caused by buoyancy, lb
C_d = drag coefficient
C_n = yawing moment coefficient
C_y = side force coefficient
D = aerodynamic drag, lb
G_{eq} = transfer function between yaw control moment and yaw control command, ft-lb
I_{xx}, I_{zz} = moments of inertia about vehicle body axes, slug-ft²
I_{xz} = product of inertia about vehicle body axes, slug-ft²
L = airship length, ft
$\mathcal{L}$ = rolling moment, ft-lb
m = mass of the airship, slug
N = yawing moment, ft-lb
$N_{\dot{v}}$ = additional yawing moment of inertia, slug-ft²
p = roll rate, rad/s
r = yaw rate, rad/s
T_{bt} = maximum available bow thrust, lb
T_1, T_2 = maximum available cruise/lift thrust, lb
$t_{1/2}$ = time to half-amplitude, s
$\bar{u}$ = control input
u, v, w = velocity components along vehicle xyz body axes, ft/s
V = airspeed of vehicle, ft/s
W = gross weight of the vehicle, lb
$\bar{x}$ = state vector
x_b, y_b, z_b = vehicle body axes with origins at center of buoyancy
x_{bt}, z_{bt} = coordinates of bow thruster location in vehicle body axes, ft
x_c, z_c = coordinates of c.m. in vehicle body axes, ft
$x_{t\delta_r}$ = moment arm of rudder control surface, ft
Y = lateral aerodynamic force in body axes, lb
$Y_{\dot{v}}$ = lateral additional mass, slug
y_{t_1}, y_{t_2} = lateral coordinates of cruise/lift thruster locations, ft
β = sideslip angle, rad
Δ = small perturbation
δ_{bt} = bow thrust throttle, %
δ_d = differential throttle of cruise/lift thruster
δ_r = rudder deflection, rad
δ_{t_1}, δ_{t_2} = throttle of cruise/lift thrusters 1 and 2, %
δ_{yc} = yaw command input, %
θ = airship pitch attitude angle, rad
θ_t = cruise/lift thrust vector angle, rad
ρ = air density, slug/ft³
τ = control effectiveness parameter
ϕ = airship roll or bank angle, rad
ψ = vehicle heading angle, rad
$\forall$ = airship envelope volume, ft³

Subscripts

bt = quantity associated with bow thruster
C/L = quantity associated with cruise/lift thruster
p, r, v = derivative with respect to p, r, or v
t_1, t_2 = quantity associated with cruise/lift thruster 1 or 2
β, δ_r = derivative with respect to β or δ_r

Superscript

$\dot{}$ = derivative with respect to time

Introduction

AIRSHIP control and maneuverability at low airspeeds have always been important aspects of its mission requirements and design. Several studies in the past have developed mathematical models[1–5] and flight dynamic simulations[6–9] to investigate the control characteristics of several advanced airship configurations.

Recent developments in control technology based on digital computers and fly-by-wire or fiber optic systems have made it realistic to consider new methods in airship design. One of the many control configured vehicle (CCV) concepts called the relaxed static stability (RSS) approach was used previously[10] to obtain a control configured, RSS airship design. It was found that conventional airship directional control criteria of being able to turn steadily at a minimum radius of two to three shiplengths could be met by a smaller than conventionally designed empennage, which has a 40% reduced fin size and having a control surface that is half of the exposed fin area. A consequence of this design is that the vehicle would have inherently less static stability and may need stability augmentation. However, the benefits of having 40% smaller fins were estimated to be a 10% reduction in vehicle aerodynamic drag and a 45% reduction in empennage weight, which can be traded for additional payload or fuel. This is indeed significant for an airship in the class illustrated here, since the reduction in empennage area translates into a 2800-lb weight reduction.

In this article, the previously mentioned RSS airship configuration is considered for which an active directional control law is synthesized by integrating powered thrusters and aero-

Received June 3, 1995; revision received April 26, 1996; accepted for publication May 2, 1996.

*Professor, Parks Campus, Department of Aerospace and Mechanical Engineering. Associate Fellow AIAA.

†Graduate Assistant, Parks Campus, Department of Aerospace and Mechanical Engineering. Member AIAA.

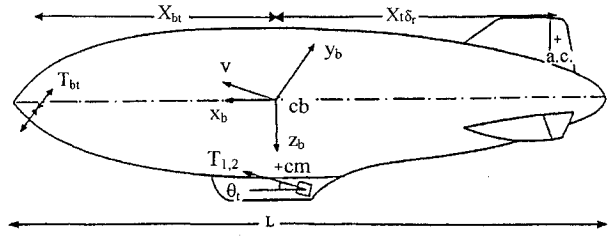

Fig. 1 RSS airship configuration and geometry.

dynamic rudder control as a function of a vehicle's airspeed. The benefits of such a control law are demonstrated by analyzing the vehicle's control and maneuverability, especially at low airspeed. Also, the dynamic stability of the RSS airship is examined to show that stability augmentation is perhaps optional since the active control provides ample control power to fly the vehicle in an open-loop fashion. The following text describes the RSS airship configuration, its lateral dynamics and control model, vehicle's stability, and the proposed active directional control law.

RSS Airship Configuration

The vehicle's configuration considered here (Fig. 1) is that of a modern airship with an inverted Y empennage and is capable of vertical/short takeoff and landing (V/STOL) flight. It is configured to have two synchronously vectorable *C/L* thrusters, symmetrically located on either side of the car. Thrust vectoring is assumed to be limited to the pitch plane, but differential thrusting is assumed to generate yaw control moment whenever possible. The airship envelope configuration was assumed to allow mounting of a bow thrusting device that can generate yaw control moment as well. For the example RSS airship illustrated here, a maximum bow thrust of ±600 lb was used. The estimated empennage geometries based on the RSS design approach are given in Table 1, whereas the corresponding aerodynamic characteristics are given in Table 2.

Table 1 Estimated physical properties of the example RSS airship

Item	Value
Airship	
Envelope volume (stretched), ft^3	2.8×10^6
Overall length, ft	460
Gross weight, lb	147,560
I_{xx}, slug-ft^2	16.2×10^6
I_{zz}, slug-ft^2	81×10^6
z_c, ft	37
Empennage	
Configuration	Inverted Y
Span, ft	126
Control surface area, ft^2	571
Fixed fin area, ft^2	569
Effective fin area caused by envelope, ft^2	2802
Total fin surface area, ft^2	3942
AR (nominal)	2.01
Propulsion/control	
Vectorable *C/L* propulsors	2 units
Nominal *C/L* thrust per unit, lb	6000
Maximum thrust at bow, lb	600
Reverse thrust	100%

Vehicle Lateral Dynamics and Control Model

The equations of lateral and directional motion were developed[1,2,6] by modeling the vehicle as a single rigid body. Basically, the airship hull was assumed to rigidly support the car, vectorable *C/L* thrusters, and bow thruster. External forces and moments acting on the airship because of gravity, buoyancy, aerodynamics, and control inputs are included in this formulation. These nonlinear equations of motion were obtained in terms of the body axes of the vehicle. They were subsequently linearized about a steady level flight condition to obtain the following linearized equations that are given in the state variable form:

$$\dot{\bar{x}} = \underline{F}\bar{x} + \underline{G}\bar{u} \tag{1}$$

where

$$\bar{x} = [\Delta v \quad \Delta p \quad \Delta\phi \quad \Delta r \quad \Delta\psi]^T$$

$$\bar{u} = \Delta\delta_{yc}$$

System matrix $\underline{F} = \underline{A}^{-1}\underline{B}$ and control input matrix $\underline{G} = \underline{A}^{-1}\underline{C}$. Matrices $\underline{A}$, $\underline{B}$, and $\underline{C}$, given later, have been developed from the linearized equations of vehicle's motion. In the control input matrix $\underline{C}$, G_{eq} is the transfer function between the yaw control moment produced and the yaw control commanded by the pilot. Consequently,

$$\Delta N_c = G_{eq}\Delta\delta_{yc} \tag{2}$$

Since there are four control devices that can produce the yaw control moment, it is assumed that

$$G_{eq}\Delta\delta_{yc} = -(T_1 y_{t_1}\cos\theta_t)\delta_{t_1} - (T_2 y_{t_2}\cos\theta_t)\delta_{t_2} + (C_{n_{\delta_r}}\rho V^2\forall/2)\delta_r + (T_{bt}x_{bt})\delta_{bt} \tag{3}$$

$$\underline{A} = \begin{bmatrix} (m - Y_{\dot{v}}) & -mz_c & 0 & (mx_c - Y_{\dot{r}}) & 0 \\ -mz_c & (I_{xx} + mz_c^2) & 0 & (I_{xz} - mz_c x_c) & 0 \\ 0 & 0 & 1 & 0 & 0 \\ (mx_c - N_{\dot{v}}) & (I_{xz} - mx_c z_c) & 0 & (I_{zz} + mx_c^2 - N_{\dot{r}}) & 0 \\ 0 & 0 & 0 & 0 & 1 \end{bmatrix}$$

$$\underline{B} = \begin{bmatrix} Y_v & mw & (W - B)\cos\phi\cos\theta & -mu + Y_r & 0 \\ 0 & -mz_c w + \mathcal{L}_p & -(Wz_c - Bz_b)\cos\phi\cos\theta & mz_c u + \mathcal{L}_r & 0 \\ 0 & 1 & 0 & \cos\phi\tan\theta & 0 \\ N_v & mx_c w + N_p & (Wx_c - Bx_b)\cos\phi\cos\theta & -mx_c u + N_r & 0 \\ 0 & 0 & 0 & \cos\phi/\cos\theta & 0 \end{bmatrix}, \quad \underline{C} = \begin{bmatrix} 0 \\ 0 \\ 0 \\ G_{eq} \\ 0 \end{bmatrix}$$

The previous equation is also constrained by the aerodynamic drag consideration since

$$T_1\cos\theta_t\delta_{t_1} + T_2\cos\theta_t\delta_{t_2} \approx D \tag{4}$$

This produces a constraint relating δ_{t_1} and δ_{t_2}. Thus, the maximum δ_d available from each *C/L* thruster, while maintaining a given forward airspeed is

$$\delta_d = 1 - [D/\{(T_1 + T_2)\cos\theta_t\}] \tag{5}$$

Table 2 Estimated aerodynamic characteristics of the example RSS airship

Aerodynamic parameter	Value/description
a_t	2.59/rad
τ	0.74
C_{n_β}	−0.865/rad
$C_{n\delta_r}$	−0.215/rad
$x_{t\delta_r}$	208 ft
C_{n_r}	−263/V/rad/s
C_{y_r}	160/V/rad/s
C_{y_β}	−0.642/rad
$Y_{\dot{v}}$	−6290 slug
$Y_r = N_{\dot{v}}$	50,919 slug-ft^2
$N_{\dot{r}}$	−46,836,078 slug-ft^2

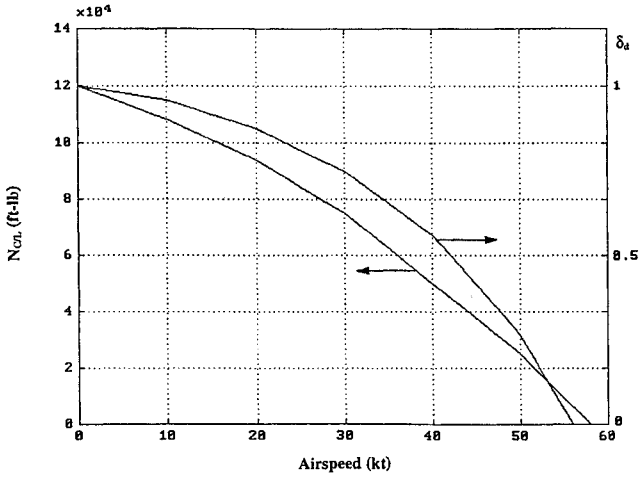

Fig. 2 *C/L* thruster yaw moment vs airspeed.

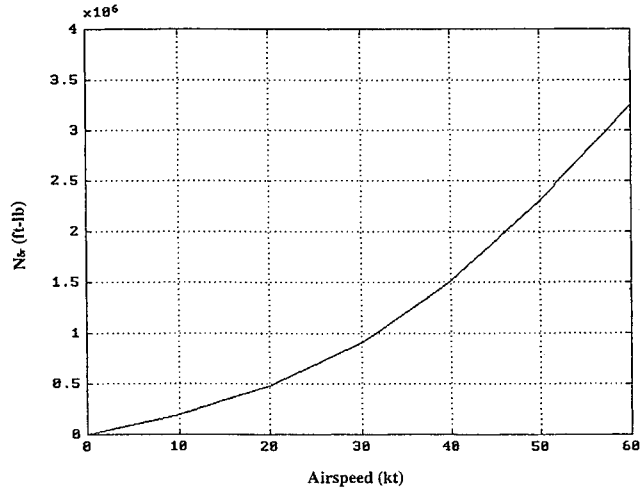

Fig. 3 Rudder yaw moment vs airspeed.

The corresponding *C/L* thruster contribution to yaw control moment, assuming $T_1 = T_2$ and $y_{t_1} = -y_{t_2}$ is

$$N_{C/L} = 2(-\cos\theta_t T_1 y_{t_1})\delta_d \tag{6}$$

Consequently, the total yaw control moment available from the four control devices is

$$N_c = 2(-T_1 y_{t_1}\cos\theta_t)\delta_d + (C_{n_{\delta r}}\rho V^2 \forall/2)\delta_r + (T_{bt}x_{bt})\delta_{bt} \tag{7}$$

Figure 2 shows the available yaw control moment by differential thrusting at various airspeeds for the example airship. The corresponding maximum moment from the bow thruster is assumed to be 126,000 ft-lb for all airspeeds, whereas that from the rudder deflected to a maximum of 25 deg is shown in Fig. 3. Maximum total yaw control moment available while using all four control devices, at various airspeeds, is given in Fig. 4. The previous state variable model of the vehicle, including the integrated yaw control moment input model, will be used next to determine its lateral/directional stability and also to develop an active directional control law.

Vehicle Stability and Directional Control

The lateral/directional stability of the example RSS airship was determined by considering the vehicle to be nominally trimmed in a steady level flight at an airspeed of 20 kn and 500 lb heaviness. Note that heaviness here is the difference between gross weight and buoyant lift of the vehicle in this flight condition. The four modes of the vehicle (Table 3) consist of 1) a rigid body rotation in yaw, 2) a weakly damped roll oscillation, 3) a coupled roll rate/yaw rate convergence,

Table 3 Vehicle lateral/directional stability modes

Mode	Eigenvalue
Rigid body yawing	0
Roll oscillation	−0.0066 ± 0.524i
Roll/yaw convergence	−0.0291
Yaw convergence	−0.2478

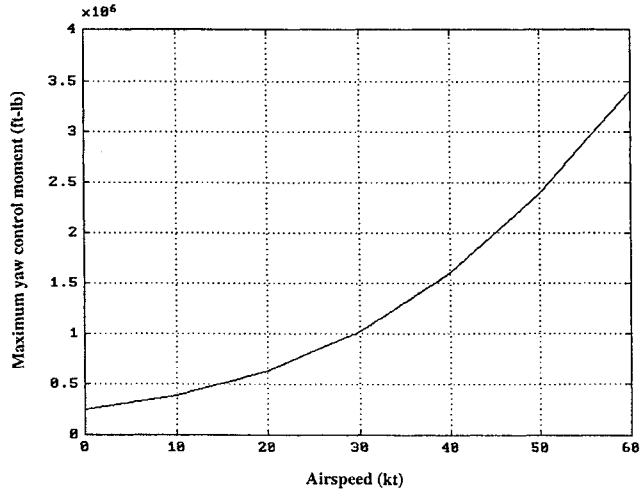

Fig. 4 Maximum available yaw control moment vs airspeed.

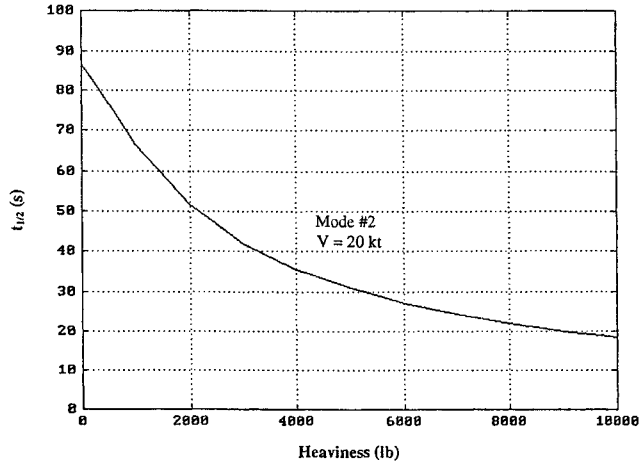

Fig. 5 Heaviness effect on roll oscillatory mode.

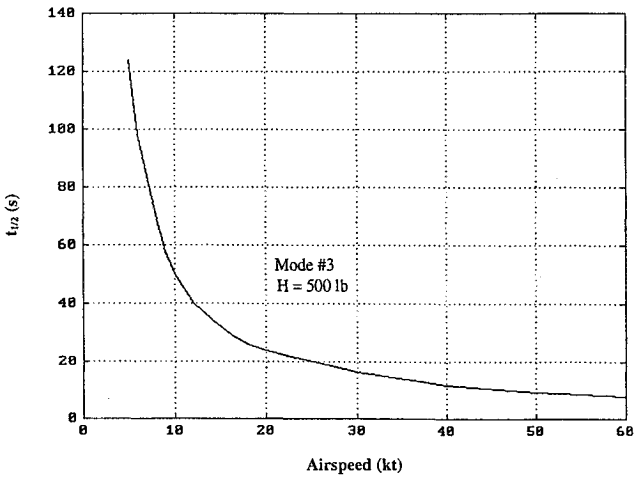

Fig. 6 Airspeed effect on roll/yaw convergence mode.

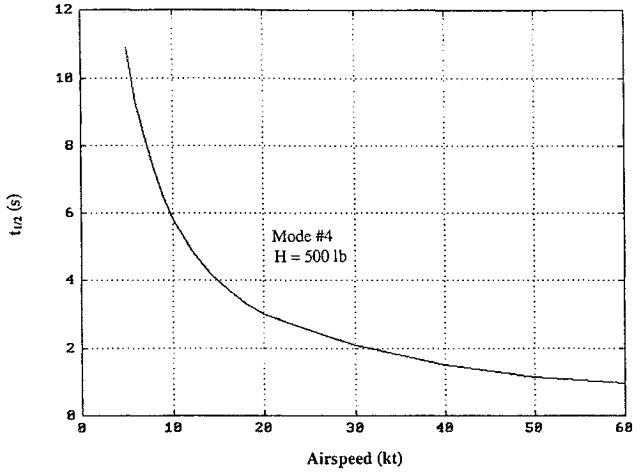

Fig. 7 Airspeed effect on yaw convergence mode.

and 4) a heavily damped yawing convergence. The roll oscillatory mode damping was found to increase significantly with an increase in heaviness (Fig. 5), whereas the time to half-amplitude $t_{1/2}$ of the roll/yaw convergence modes decreased rapidly with increasing airspeed (Figs. 6 and 7), because of increased aerodynamic damping.

Typical vehicle's response to a 10 ft/s lateral velocity disturbance while flying at 5 kn (≈8 ft/s) airspeed (Fig. 8) indicates a corresponding change in vehicle's yaw rate up to 1 deg/s and heading drift over 180 deg. A full rudder deflection of −25 deg under the same conditions resulted in the vehicle developing a steady yaw rate of 0.5 deg/s (Fig. 9). Clearly, the rudder control alone is inadequate in such a case to overcome the disturbance effects. These results indicate that although the vehicle is dynamically stable at all airspeeds, it is likely to respond more to disturbances at low airspeeds and could use greater control power at airspeeds below 15 kn where aerodynamic controls are ineffective.

Accordingly, it is proposed to use the bow thruster and the differential thrust from the *C/L* propulsors to generate yaw control moment at airspeeds below 30 kn. The effect of including these devices, in addition to the rudder control, on the vehicle directional dynamics is illustrated in Figs. 10a and 10b while the vehicle is operating at an airspeed of 5 kn and 500 lb heaviness. It is observed that all three yaw control devices cumulatively produced a yaw rate of 2 deg/s, whereas rudder plus *C/L* thrusters produced a yaw rate of 1 deg/s. Further, rudder alone is practically ineffective in such a case. Consequently, the vehicle's maneuverability at low airspeeds below 15 kn is possible only with augmenting the rudder with these powered controls. An active approach to synthesizing the vehicle's yaw control using the previous control devices is discussed next.

Active Directional Control Law

It is observed that the advantage of producing yaw control moment by using powered thrust controls diminishes with increasing airspeed (Fig. 11) as the rudder becomes more powerful, especially at airspeeds above 30 kn. Consequently, an active control law is proposed that fully utilizes the powered thrust controls at low airspeeds below 15 kn and gradually transitions by reducing the powered thrust over the airspeed range of 15–30 kn. At an airspeed above 30 kn, the control law calls for pure aerodynamic yaw control moment from the

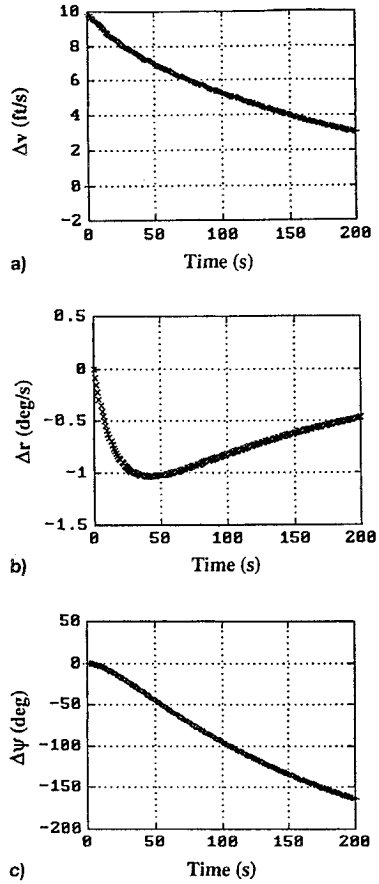

Fig. 8 Vehicle response to a 10 ft/s lateral velocity disturbance: a) Δv, b) Δr, and c) $\Delta\psi$ vs time.

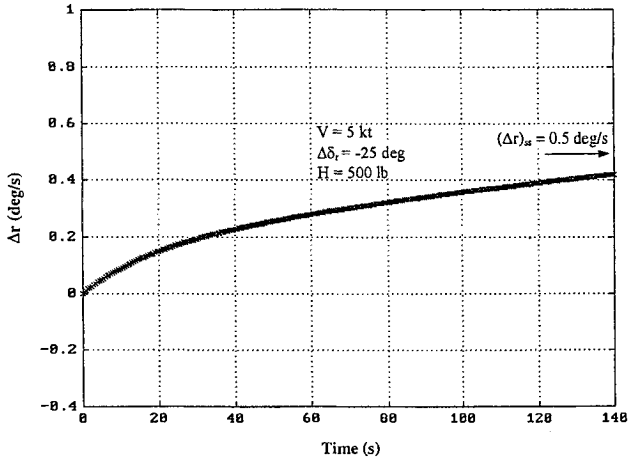

Fig. 9 Vehicle response to rudder control input.

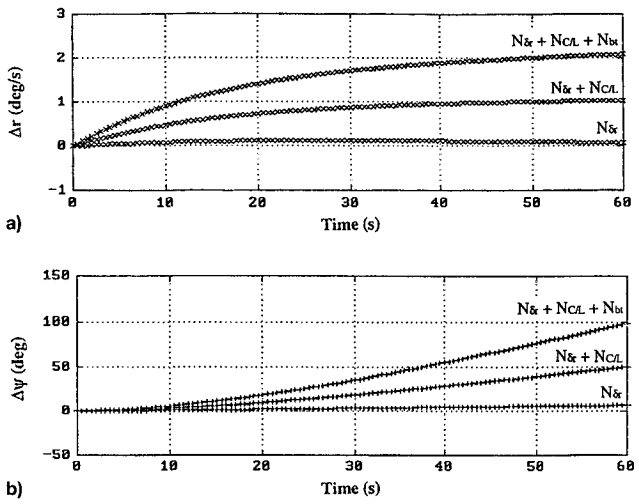

Fig. 10 Directional maneuverability with augmented yaw control: a) Δr and b) $\Delta\psi$ vs time.

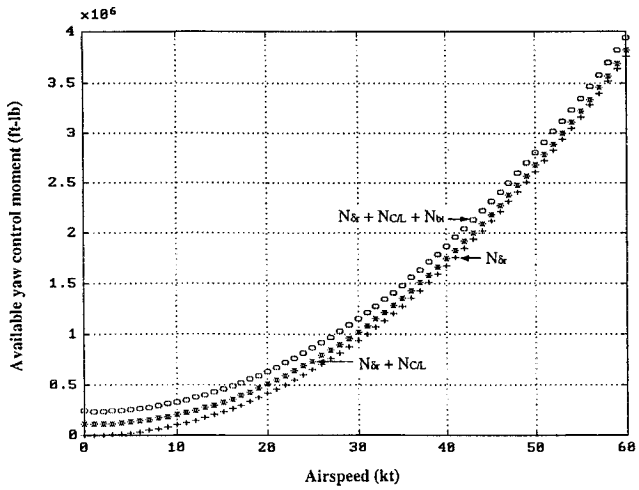

Fig. 11 Available yaw control moment vs airspeed.

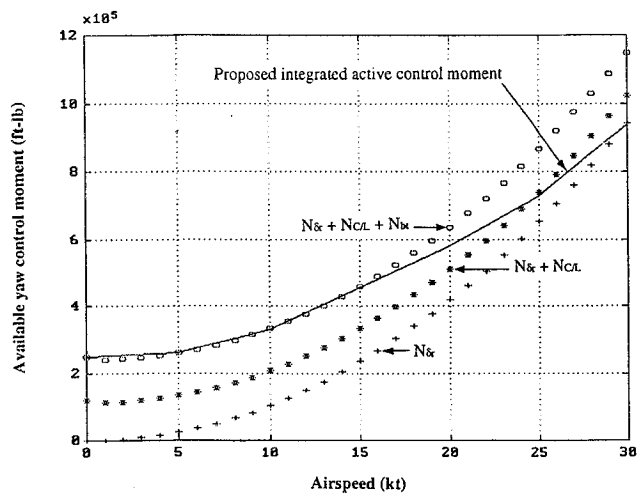

Fig. 12 Integrated yaw control moment vs airspeed.

rudder alone. This sequence of events is illustrated in Fig. 12, which indicates a smooth change in total available yaw control moment from hover through 30 kn. The corresponding schedule for thrust controls as a function of airspeed is specified in Table 4.

The active control law proposed previously was implemented in a digital flight simulation, where the vehicle was

Table 4 Bow thrust and *C/L* thrust schedule for yaw control

Airspeed, kn	N_{bt}, %	$N_{C/L}$, %	N_{δ_r}, %
15	100	100	100
16	88.23	100	100
17	77.46	100	100
18	64.69	100	100
19	52.92	100	100
20	41.15	100	100
21	30.86	100	100
22	20.57	100	100
23	10.29	100	100
24	0	100	100
25	0	83.33	100
26	0	66.66	100
27	0	50	100
28	0	33.33	100
29	0	16.67	100
30	0	0	100

Table 5 Time to maneuver the airship through a 90-deg turn

Airspeed, kn	Proposed active yaw control, s	Conventional rudder control, s
0.2	60	—
3	90	—
5	129	900
10	132	500
15	136	360
20	141	200
25	145	180
30	150	150

required to maneuver through a 90-deg turn, at various airspeeds (Table 5). The corresponding time to perform this maneuver was compared with that using a conventional rudder alone. It was found that the proposed active control law significantly improved the directional control and maneuverability, particularly at airspeeds below 20 kn. Further, it also provided excellent directional control near hover, which was nonexistent in a vehicle with rudder control alone.

It is expected that the proposed active directional control law can be implemented in the flight control system and can be made transparent to the pilot. Consequently, the vehicle now has directional control from zero airspeed or hover through cruise speed, which can be utilized via the pilot's directional control input to a sidestick or pedals.

Concluding Remarks

Significant improvement in directional control and maneuverability of a modern airship can be realized by considering powered thrust controls for generating yaw control moment at low airspeeds. An active control law that generates a yaw command to activate the rudder and powered thrust control devices has been formulated such that it can be implemented in a digital fly-by-wire/light flight control system. Although a bow thruster was considered in the present study, a stern thruster could instead be used in the proposed active control law. It is observed that providing lateral/directional control at low airspeeds would make a modern airship a more effective, hover-capable V/STOL vehicle. Future studies in this area should perhaps consider implementation issues through flight simulator studies and hardware development.

References

[1]Clark, J. W., "Derivation and Application of Equations of Motion for Buoyant and Partially-Buoyant Air Vehicles," NADC TM VT-TM-1716, Feb. 1976.

[2]Nagabhushan, B. L., "Equations of Motion of a Heavy Lift Airship with a Simply Suspended Payload," Goodyear Aerospace Corp.,

GER 16443, Akron, OH, March 1977.

[3]Nagabhushan, B. L., and Tomlinson, N. P., "Flight Dynamics Simulation of a Heavy Lift Airship," *Journal of Aircraft*, Vol. 18, No. 2, 1981, pp. 96–102.

[4]Jones, S. P., and Krausman, J. A., "Nonlinear Dynamic Simulation of Tethered Aerostat," *Journal of Aircraft*, Vol. 19, No. 8, 1982, pp. 679–686.

[5]Nagabhushan, B. L., and Pasha, R. K., "Analysis of Airship Lateral Maneuverability," *Journal of Aircraft*, Vol. 29, No. 3, 1992, pp. 299, 300.

[6]Tischler, M. B., Jex, H. R., and Ringland, R. F., "Simulation of Heavy Lift Airship Dynamics over Large Ranges of Incidence and Speed," AIAA Paper 81-1335, July 1981.

[7]Talbot, P. D., Miura, H., and Tucker, G. E., "Piloted Simulation of a Buoyant Quad-Rotor Aircraft," AIAA Paper 81-1345, July 1981.

[8]Nagabhushan, B. L., and Faiss, G. D., "Thrust Vector Control of a V/STOL Airship," *Journal of Aircraft*, Vol. 21, No. 6, 1984, pp. 408–412.

[9]Nagabushan, B. L., and Tomlison, N. P., "Thrust Vectored Take-Off, Landing and Ground Handling of an Airship," *Journal of Aircraft*, Vol. 23, No. 3, 1986, pp. 250–256.

[10]Nagabhushan, B. L., "Control Configuration of a Relaxed Stability Airship," *Journal of Aircraft*, Vol. 28, No. 9, 1991, pp. 558–563.